ACS APPLIED MATERIALS & INTERFACES

Research Article

www.acsami.org

# Effective End Group Modification of Poly(3-hexylthiophene) with Functional Electron-Deficient Moieties for Performance Improvement in Polymer Solar Cell

Chi-Min Chen, Tzu-Hao Jen, and Show-An Chen*

Department of Chemical Engineering and Frontier Research Center on Fundamental and Applied Sciences of Matters, National Tsing-Hua University, Hsinchu 30013, Taiwan, Republic of China

Supporting Information

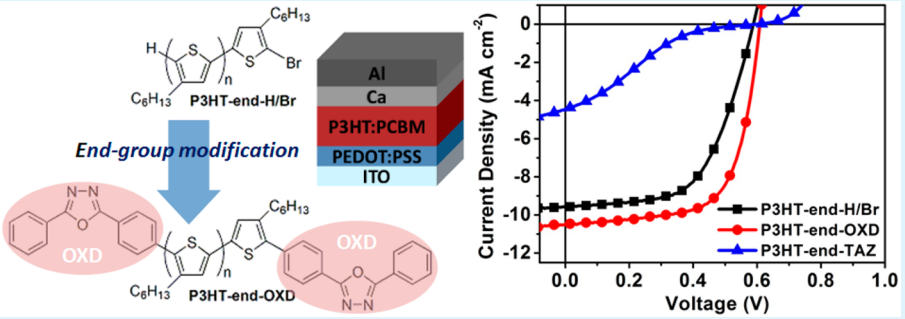


**ABSTRACT:** A series of end-functionalized poly(3-hexylthiophene)s (P3HTs) were synthesized by end-capping with electron-deficient moieties (EDMs, oxadiazole (OXD) and triazole (TAZ)) to prevent the negative influence of bromine chain ends in the common uncapped P3HT in polymer solar cell (PSC) applications. On the basis of the electron-withdrawing capability of the planar OXD end groups, P3HT-end-OXD relative to the uncapped P3HT exhibits a raised absorption coefficient, extended exciton lifetime, and increased crystalline order in the blend with PCBM, leading to an effectual improvement in photovoltaic parameters. However, P3HT-end-TAZ has an opposite result even worse than that of the uncapped P3HT, arising from bulky TAZ end groups. As a consequence, P3HT-end-OXD gives a power conversion efficiency (PCE) of 4.24%, which is higher than those of the uncapped P3HT (3.28%) and P3HT-end-TAZ (0.50%). The result demonstrates that the EDM modification is a valuable method to tailor the structural defect of polymer chain ends. However, the efficacy is dependent on the structure of EDM.

**KEYWORDS:** *end group modification, polymer chain ends, poly(3-hexylthiophene), electron-deficient moiety, electron-withdrawing capability, polymer solar cell*

## INTRODUCTION

Conjugated polymers have received considerable attention as semiconductors for applications in organic optoelectronic devices by virtue of their ease of fabrication, promising flexibility, and solution processability.[1,2] Regioregular poly(3-hexylthiophene) (rr-P3HT) is the most representative conjugated polymer having the advantages of self-assembly ability and desirable sunlight harvesting characteristics (absorption of light up to 650 nm with high absorption coefficient), and consequently it has been investigated for applications in polymer thin-film transistor (PTFTs) and bulk heterojunction (BHJ) polymer solar cells (PSCs), for which benchmark hole mobility ($\mu_h$) of amorphous silicon (0.1 $cm^2$ $V^{-1}$ $s^{-1}$)[3] and an excess of 5% in power conversion efficiency (PCE)[4−6] have been achieved, respectively.

P3HTs with high regioregularity (RR) are usually prepared using the MuCullough method,[7] Rieke zinc (Zn*) mediated method,[8] and Grignard metathesis (GRIM) method[9] by regiocontrol of organometallic intermediates from 2,5-dibromo-3-hexylthiophene monomers. Syntheses via these methods all yield uncapped P3HTs with the end group composition, one end with hydrogen and the other end with bromine, originating from methanol quenching after polymerization.[10] The structural defect of bromine chain ends was found to be regarded as impurity sites in the photoactive layer, giving rise to an influence in PSC performance by the disturbance of chain packing, trapping of a charge carrier, quenching of photogenerated excitons, or unfavorable film morphology, even though the end group content is rather low relative to the repeat unit (3-hexythiophene) of the P3HT.[11−15] Furthermore, the other report also suggested that the small concentrations of residual reactive end groups in polymer chain ends would make PSC more sensitive to photoactive layer thickness and thermal degradation, affecting the device stability adversely.[16]

Received: April 17, 2015
Accepted: August 24, 2015
Published: August 24, 2015





DOI: 10.1021/acsami.5b03213
ACS Appl. Mater. Interfaces 2015, 7, 20548−20555

**Scheme 1. Molecular Structures of P3HTs and Their Corresponding End Groups**

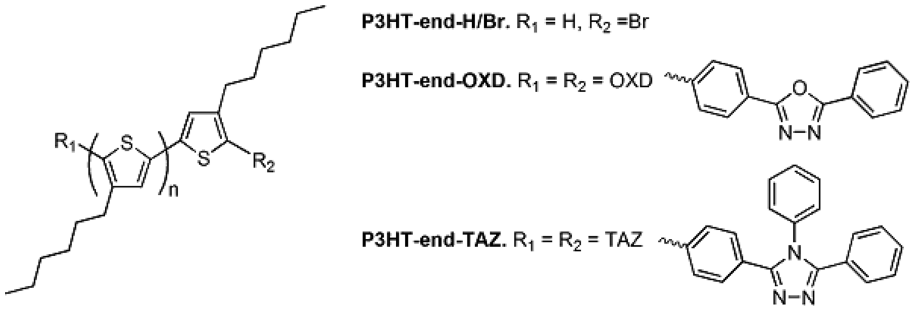


On the other hand, end-functional-group-modified P3HTs were found to be able to enhance the efficiency or stability of PSC resulting from improved bicontinuous network morphology in P3HT with CdSe quantum rods[11] or P3HT with PCBM[14,15] composite films. Phase separation between donor and acceptor in the blends is an essential factor for a PSC to function because exciton dissociation can mainly occur by charge transfer at the donor−acceptor (D−A) interface and the generated electrons and holes are conducted toward the cathode and anode via their respective channels.[17−19] However, exciton diffusion length in conjugated polymers is extremely short on the order of 10 nm, which is disadvantageous for exciton migration to an interface of D−A within its lifetime, namely an unexpected exciton decay is possibile.[18,19]

Since exciton diffusion length depends on both the mobility and lifetime of an exciton, a longer lifetime could contribute an increased diffusion length to the exciton.[20] Yang and Shao suggested that the inclusion of an appropriate organic small molecule with a long exciton lifetime in the photoactive layer is conducive to improving PSC performance.[21] The Müller-Buschbaum group also presented an increased effective exciton lifetime induced by strong spin−orbit coupling through the doping of heavy metal nanoparticles, which can lend support to further enhance the efficiency of the P3HT:PCBM solar cells.[22] Additionally, in our previous work, grafted oxadiazole (OXD) on the end of the side chain on poly[2-methoxy-5-(2′-ethylhexyloxy)-1,4-phenylenevinylene] (MEH-PPV) or poly-(9,9-dioctylfluorene) (PFO) by a nonconjugated decyloxy group as a spacer can promote exciton dissociation and electron transport, which may reflect a potentiality on improvement of PCE by such modification.[23] Another effort of incorporation of electron-deficient moieties (EDMs, OXD or triazole (TAZ)) as end-cappers in PFO as the emitting layer in polymer light emitting diodes (PLEDs) can induce a minor amount of extended conjugation length species (more order structure regarded as $\beta$-phase)[24] near chain ends to promote energy transfer from an amorphous matrix to the $\beta$ phase for more efficient device performance.[25,26]

On the basis of these considerations, here we propose a simple way for P3HT via end-capping EDM, such as OXD and TAZ (Scheme 1), to investigate characteristic differences and optoelectronic influence in photovoltaic devices relative to those of the common uncapped P3HT. The end-functionalized P3HT with OXD in chain ends, P3HT-end-OXD, as a donor exhibits the best PSC of 4.24% among the three P3HT:PCBM blends due to an effectual increase in short-circuit current density ($J_{sc}$) and fill factor (FF) of the resulting PSC. The improvement of device efficiency is attributed to the raised absorption coefficient and extended exciton lifetime for photocurrent creation and better chain ordering for effective charge carrier transport, originating from the electron-withdrawing capability of the planar OXD end groups. The results indicate that the structural defect of the polymer chain ends is a non-negligible influence on PSC performance but can be tailored by a fine modification with appropriately functional EDMs.

## EXPERIMENTAL SECTION

**Materials and Synthesis.** All materials and reagents were purchased from commercial sources and used without further purification. All reactions were conducted under a nitrogen atmosphere using standard Schlenk line techniques or in a nitrogen-filled glovebox. *N*′-Benzoyl-4-bromobenzohydrazide (**1**),[25] 2-(4-bromophenyl)-5-phenyl-1,3,4-oxadiazole (OXD-Br),[25,27] 3-(4-bromophenyl)-4,5-diphenyl-1,2,4-triazole (TAZ-Br),[25,28] uncapped P3HT (designated as P3HT-end-H/Br),[9] and end-functionalized P3HTs (P3HT-end-OXD and P3HT-end-TAZ)[29] were prepared according to the literature, and their synthetic procedures are described in detail in the SI (Schemes S1 and S2).

**General Instrumentation.** The $^1$H NMR and the EI-MS spectra were carried out on a Varian Unity Inova 500 NMR spectrometer in deuterated solvent and a MAT-95XL high resolution mass spectrometer (HRMS) using an electron impact ionization procedure, respectively, in the NSC Regional Instrument Centre at National Tsing Hua University, Taiwan. The gel permeation chromatography (GPC) was measured using HPLC grade THF as an eluent at a flow rate of 1.0 mL min$^{-1}$ in 7.8-mm-i.d. and 300-mm-long Styragel HR2, 3, and 4 columns in series (Waters) at 40 °C to analyze molecular weight distributions and polydispersity indices (PDI) of polymers relative to polystyrene standards from a Waters 2481 UV detector and Waters 2410 RI detector. The calibration curve was determined by using 10 specified standards with molecular weights ranging from 1360 to 1.29 × 10$^6$ kDa. UV−vis absorption spectra were taken on the thin films cast onto quartz glasses by using a PerkinElmer Lambda 35 spectrophotometer. Density functional theory (DFT) calculation for the chain conformation is performed using the Gaussian 09 package at the B3LYP/6-31G* level.[30] The X-ray photoelectron spectroscopy (XPS) and ultraviolet photoelectron spectroscopy (UPS) spectra were obtained with a VG Multilab 2000 instrument under a pressure of 1 × 10$^{-9}$ mbar using monochromatized Mg (K$\alpha$) X-rays ($h\nu$ = 1254.6 eV) and He I radiation ($h\nu$ = 21.22 eV) as the light source, respectively. The highest occupied molecular orbital (HOMO) level of each P3HT is determined from the result of UPS along with the following equation, HOMO level = $h\nu$ − ($E_{cutoff}$ − $E_{onset}$), where $E_{cutoff}$ and $E_{onset}$ are the turning points at high and low binding energy regions, respectively. The P3HT samples


DOI: 10.1021/acsami.5b03213
ACS Appl. Mater. Interfaces 2015, 7, 20548−20555

for XPS and UPS analyses were spin-coated on ITO glasses from their polymer solutions in *o*-DCB (10 mg $mL^{-1}$) under a nitrogen-filled glovebox and annealed at 110 °C for 10 min after solvent annealing. Time-resolved photoluminescence (TR-PL) spectroscopy of P3HT films on cleaned ITO substrates were analyzed by a time-correlated single photon counting (TCSPC) system with a microchannel plate photomultiplier tube (Hamamatsu Photonics R3809U-50) and a spectrometer (Edinburgh, Lifespec-ps with TCC900 data acquisition card). The measurement was proceeded with a pulse laser of 405 nm for excitation (P3HT-end-H/Br, -OXD, and -TAZ have $\lambda_{max}$ at 555, 555, and 518 nm, respectively) and collected at 650 nm. The predetermined number of counts for each collection of emission decay was set for 3000 counts. The transmission electron microscopy (TEM) images were recorded on a JEOL JEM-2100 transmission electron microscope operating at 200 kV. The TEM samples of P3HT:PCBM blend films were prepared previously by spin-coating onto ITO/PEDOT:PSS substrates in accordance with the PSC fabrication process and transferred on top of a Cu grid covered with a carbon film through floating on deionized water and then followed by evaporation of the solvent in a desiccator under a vacuum. Grazing-incidence wide-angle X-ray scattering (GIWAXS) was conducted on beamline 17A1 of the National Synchrotron Radiation Research Center (NSRRC), Taiwan, with a wavelength of 1.321 Å and constant incidence angle of 0.15° on the P3HT:PCBM blend films spin-cast onto Si/PEDOT:PSS substrates in accordance with the PSC fabrication process. All the thicknesses of films were determined by a Tencor P-10 profilometer.

**Hole-Only Device Fabrication and Characterization.** The hole-only devices were manufactured by casting the P3HT:PCBM blend films onto the ITO/PEDOT:PSS substrates with the post-treatment as a PSC fabrication process, and then Au electrodes with a thickness of 60 nm were thermally evaporated on top of the photoactive layer. All devices were measured in a nitrogen-filled glovebox using a Keithley 238 source measure unit (SMU). The hole mobilities can be estimated precisely by fitting the dark current versus voltage curves for hole-only devices with a single-carrier space charge limited current (SCLC) model using the following formula: $J = 9\varepsilon_0\varepsilon_r\mu V^2/8L^3$, where $\varepsilon_0$ is the permittivity of free space, $\varepsilon_r$ is the dielectric constant of the materials, $\mu$ is the carrier mobility, and $L$ is the thickness of the film. The applied bias voltage for a device is corrected for the built-in potential ($V_{bi}$) across its photoactive layer so that $V = V_{applied} - V_{bi}$.[31]

**PSC Fabrication and Performance Measurement.** ITO glasses were used as the anodes and cleaned stepwise in detergent aqueous solution, deionized water, isopropyl alcohol, and acetone. The cleaned ITO glasses were exposed on oxygen plasma at a power of 50 W under a pressure of $1.93 \times 10^{-1}$ Torr for 5 min. PEDOT:PSS (Clevios P VP AI 4083, 1.5 wt % in water) layers with a thickness of 30 nm were spin-coated on the oxygen plasma-treated ITO glasses and then baked at 140 °C for 10 min under a vacuum as the hole injection layer. On top of PEDOT:PSS layers, P3HT:PCBM (1:0.8 w/w) films (200 nm) were spin-coated from their blend solutions in *o*-DCB at a concentration of 36 mg $mL^{-1}$ and dried within covered glass Petri dishes. After solvent annealing, the resulting films were annealed at 110 °C for 10 min. All processes were carried out in a glovebox with nitrogen, except these two steps for ITO cleaning and PEDOT:PSS coating. Finally, the PSC fabrication was completed by thermal evaporation of a thin layer of Ca (about 8 nm) covered with a layer of Al (100 nm) as a cathode through a shadow mask under a pressure of $2 \times 10^{-6}$ Torr. The active area of the devices is approximately 0.06 $cm^2$. The current density−voltage ($J$−$V$) characteristics of the PSCs were measured using a Keithley 2400 source measure unit (SMU) while illuminated under AM1.5G illumination at an intensity of 100 mW $cm^{-2}$ from a San-Ei XES-40S2, 150 W solar simulator in a nitrogen-filled glovebox. The external quantum efficiency (EQE) spectra were collected by using a QE-R system (Enlietch, Taiwan) with monochromatic light from an Oriel 150 W xenon lamp passing through a monochromator onto the unencapsulated PSCs under air.

## RESULTS AND DISCUSSION

**Material Synthesis and Characterization.** The molecular structures of P3HT-end-H/Br, end-functionalized P3HTs, and their individual end groups are shown in Scheme 1. To avoid a disturbance to intrinsic chain packing of P3HT by modified chain ends, the EDMs without *tert*-butyl groups were used as end-cappers here and synthesized following the reported methods.[25,27,28] P3HTs were controlled with a high RR and appropriate molecular weight (~50 kDa) to maintain the original absorption capability, chain packing, and electric properties of rr-P3HT for efficient device performance.[12,32−34] The P3HT-end-H/Br was polymerized via the GRIM method[9] and converted to end-functionalized P3HTs with EDMs in chain ends by an in situ method through subsequent addition of Grignard reagent with end-capper for the termination reaction (OXD for P3HT-end-OXD and TAZ for P3HT-end-TAZ).[29] All P3HTs were purified by Soxhlet extraction and then reprecipitated with methanol. As listed at Table 1, RR and molecular weight distribution of three P3HTs are nearly identical, such that these two factors affecting the PSC performance can be excluded, accomplishing a fair competition in the structural differences of end groups.[32−34] Besides, the success of the end group conversion was confirmed by elemental composition using XPS. Compared to P3HT-end-H/Br with the remained Br 3d signal, the new peaks in the range of N 1s are only observed in two end-functionalized P3HTs, as shown in Figure S1.

**Table 1. Physical Properties of P3HTs Used in This Work**

| P3HTs | RR (%) | $M_n$ (kDa) | PDI | DP[a] |
|---|---|---|---|---|
| P3HT-end-H/Br | 99.4 | 38.4 | 1.8 | 230.4 |
| P3HT-end-OXD | 99.3 | 40.0 | 1.8 | 237.9 |
| P3HT-end-TAZ | 98.8 | 40.6 | 1.7 | 240.6 |

[a]Degree of polymerization is estimated from the following formula, $DP = (M_{n,polymer} - 2 \times M_{w,end\text{-}group})/M_{w,repeat\text{-}unit}$. The $number_{end\text{-}group}$ of P3HT-end-OXD and -TAZ is 2 by reason for these end-cappers with aryl structure.[29] The molecular weight ($M_w$) of the end group in P3HT-end-H/Br is 1.01 Da for the H atom and 79.90 Da for the Br atom. The $M_w$ of the OXD end group is 221.23 Da, and the $M_w$ of the TAZ end group is 296.34 Da. The repeat unit of P3HT is 3-hexylthiophene, having a $M_w$ of 166.28 Da.

**Optical and Electronic Properties.** The UV−vis absorption spectra of spin-cast thin films of P3HTs and their blends with PCBM are shown in Figure 1, and the corresponding characteristic data are summarized in Table 2. For the pristine P3HT films, P3HT-end-TAZ exhibits the weakest absorption coefficient profile under the same thickness of 200 nm (especially on the shoulder 603 nm associated with


DOI: 10.1021/acsami.5b03213
ACS Appl. Mater. Interfaces 2015, 7, 20548−20555

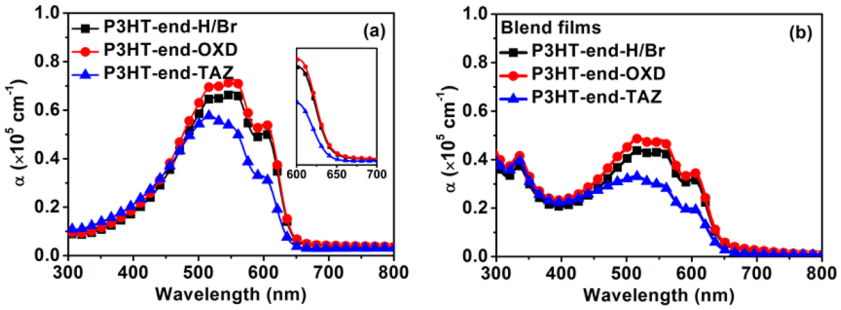


**Figure 1.** Optical absorption spectra of P3HTs: (a) pristine films (the inset shows a magnified range of 600 to 700 nm) and (b) blend films with PCBM.

**Table 2. Optical Properties and Molecular Energy Levels of P3HTs**

| P3HTs | $\lambda_{max}$ (nm)[a] | $\lambda_{onset}$ (nm)[a] | $E_g^{opt}$ (eV)[b] | HOMO (eV)[c] | LUMO (eV)[d] |
|---|---|---|---|---|---|
| P3HT-end-H/Br | 554 | 643 | 1.93 | −5.32 | −3.39 |
| P3HT-end-OXD | 554 | 643 | 1.93 | −5.47 | −3.54 |
| P3HT-end-TAZ | 517 | 636 | 1.95 | −5.40 | −3.45 |

[a]Determined from absorption spectra of P3HTs in pristine films. [b]$E_g^{opt}$ determined from the onset of absorption spectra in pristine films. [c]Evaluated by UPS. [d]Calculated by the equation: LUMO = HOMO + $E_g^{opt}$.

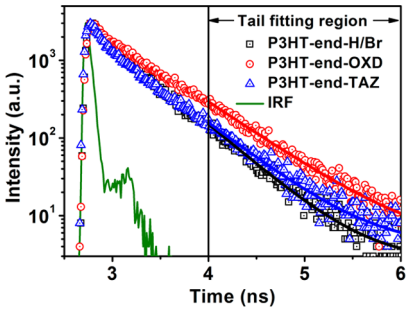


**Figure 2.** TR-PL decay curves of P3HT films monitored at 650 nm. Here, the green curve is the IRF, and the solid lines at times of 4−6 ns are single exponential tails fit to the data for each sample.

the interchain interaction)[35,36] with the highest extent of blue-shifts at maximum absorption ($\lambda_{max}$) and absorption onset ($\lambda_{onset}$) among the three P3HTs. The result arises from looser interchain packing imparted by the steric hindrance of TAZ end groups and, therefore, can bring about decreased absorption.[13] However, the characteristic absorption band of P3HT-end-OXD is identical to that of P3HT-end-H/Br, yet the former has a slightly higher absorption coefficient than the latter, allowing a promotion of more exciton generation by photoexciation.[13,32] The optical band gap ($E_g^{opt}$) determined from the $\lambda_{onset}$ (the inset in Figure 1a) for P3HT-end-TAZ of 1.95 eV is slightly higher by 0.02 eV than those of P3HT-end-H/Br and -OXD, which can be also ascribed to the interruption of $\pi$-conjugation by bulky TAZ end groups. For the blend films with PCBM (Figure 1b), the absorption trend is similar to that in the cases of a polymer alone. The HOMO levels of P3HTs were estimated by ultraviolet photoelectron spectroscopy (UPS), as shown in Figure S2. P3HT-end-OXD has the HOMO level −5.47 eV lower than those of P3HT-end-H/Br (−5.32 eV) and -TAZ (−5.40 eV), resulting in a slightly enhanced $V_{oc}$ of its PSCs, as mentioned below. Using the values of HOMO level and the $E_g^{opt}$, the values of lowest unoccupied molecular orbital (LUMO) levels of P3HT-end-H/Br, -OXD, and -TAZ were calculated to be −3.39, −3.54, and −3.45 eV, respectively.

**Fluorescence Quenching Effect.** In view of the presence of $\pi$-delocalization between EDMs and nearly 3-hexylthiophene units in end-functionalized P3HTs, we also perform TR-PL spectroscopy to identify subtle differences of exciton lifetimes ($\tau$) in P3HTs. Figure 2 shows the individual emission decay curves of pristine P3HT films with single exponential tail fits in the time range of 4 to 6 ns for exclusion of effects of the instrument response function (IRF). Compared to P3HT-end-TAZ with 466 ps, the measured PL lifetime of P3HT-end-OXD was increased by more than 27% from P3HT-end-H/Br of 411 to 524 ps. Aside from the removal of the exciton quencher bromine end groups, the other possible grounds for extended exciton lifetime in end-functionalized P3HTs was the improved coplanarity of successive 3-hexylthiophene units near chain ends due to electron-withdrawing capability of EDMs as revealed below.[13] Therefore, photoexcitons in such minor amounts of conjugated species at chain ends will probably transfer to longer conjugated species, giving rise to an increase in exciton lifetime. This behavior is analogous to a MEH-PPV single chain system, in which two to three chromophores with different conjugation lengths appear and the exciton of short conjugation length can transfer its energy to that of longer conjugation length species before emission.[37] For these reasons, the fine modification of P3HT by the incorporation of EDMs onto chain ends can increase exciton lifetime, which in turn provides more chance for excitons to travel to the P3HT and PCBM interface in the photoactive layer for exciton dissociation.[20]

**Film Morphology.** To examine the influence of PCBM distribution within the thin films of end-functionalized P3HTs with EDM end groups, the blend films are examined by TEM to probe the extent of phase separation between P3HT and PCBM. In their TEM images, relatively dark regions represent PCBM-rich domains for the reason that PCBM has higher density (1.50 g $cm^{-3}$)[38] than P3HT (1.10 g $cm^{-3}$).[39] In contrast to P3HT-end-H/Br:PCBM and P3HT-end-OXD:PCBM blend films with identical homogeneous morphologies, P3HT-end-TAZ:PCBM blend film exhibits relatively blurred bicontinuous phase with some isolated PCBM aggregations, leading to deterioration in PSC performance.[33] The reasonable ground for such appearance is the presence of additional space created by poor intermolecular stacking due to nonplanar TAZ end groups, where more PCBM molecules can be accommodated, as shown in Figure 3.


DOI: 10.1021/acsami.5b03213
ACS Appl. Mater. Interfaces 2015, 7, 20548−20555

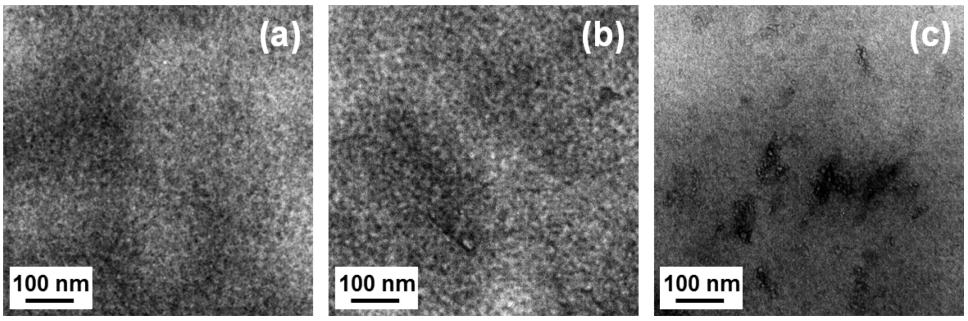


**Figure 3.** TEM images of (a) P3HT-end-H/Br:PCBM, (b) P3HT-end-OXD:PCBM, and (c) P3HT-end-TAZ:PCBM blend film morphology.

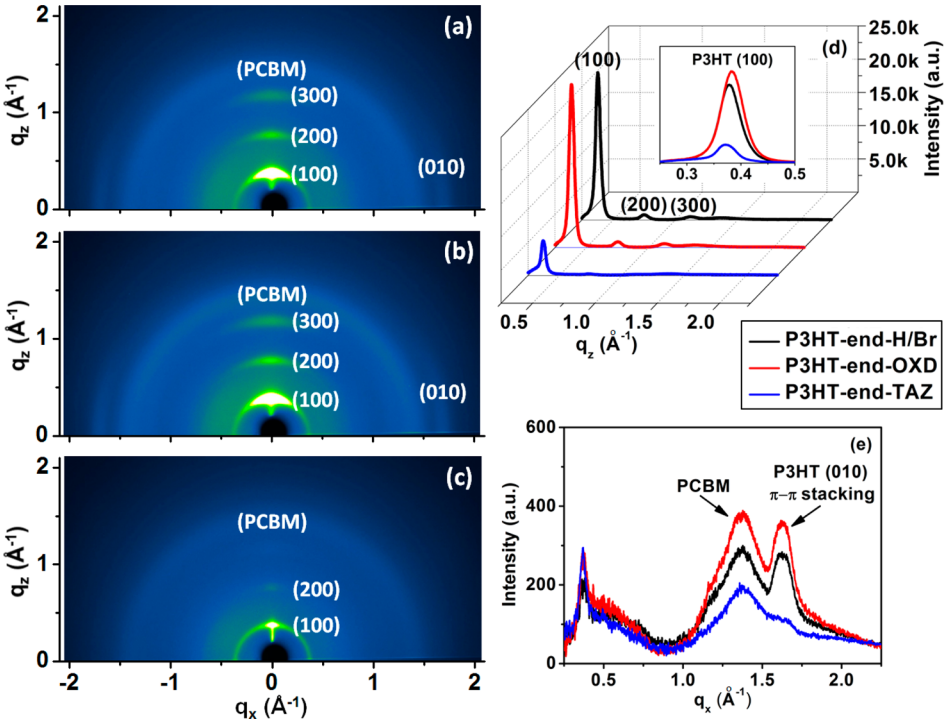


**Figure 4.** 2D GIWAXS patterns of (a) P3HT-end-H/Br:PCBM, (b) P3HT-end-OXD:PCBM, and (c) P3HT-end-TAZ:PCBM blend films. The corresponding integrated 1D diffractograms along (d) out-of-plane and (e) in-plane scattering geometry from 2D GIWAXS patterns. The inset in d shows a magnified range of 0.25 to 0.5 Å$^{-1}$.

**Polymer Chain Conformation and Molecular Order.** The minimum-energy chain conformations of the three P3HTs were verified by DFT method using the simplified model of methyl-substituted tetrathiophene (designated as Tetramer) to investigate the effect of EDM end groups in backbone coplanarity of end-functionalized P3HTs relative to P3HT-end-H/Br. The calculations were carried out using the Gaussian 09 programs with the B3LYP/6-31G* basis set; the results are shown in Figure S3. Compared to tetramer-end-TAZ, the optimized molecular conformation of tetramer-end-OXD has smaller dihedral angles in most thiophene−thiophene linkers than tetramer-end-H/Br. The simulation result indicates the backbone of P3HT-end-OXD can be induced with a better extent of coplanarity by electron-withdrawing OXD end groups than P3HT-end-H/Br, which can promote interchain packing for efficient hole transport.[40,41] In addition, since the phase separation correlates well with the nanoscale organization for both components, the blend films are also characterized by GIWAXS to explore interchain packing of P3HTs and molecular ordering of PCBM.[42] The 2D GIWAXS patterns (Figure 4a−c) with a series of out-of-plane (h00) diffraction arcs and a slight in-plane (010) diffraction arc demonstrate that all P3HTs in blend films have a well-organized lamellar structure oriented normal to the substrate as reported in the literature for P3HT:PCBM blends.[32,33] However, polymer chains of each of the three P3HTs exhibit different degrees of ordering in their blends, as evidenced by their diffraction intensities. From the integrated diffraction patterns along $q_z$ and $q_x$ directions (Figure 4d and e), the distinct differences of (100) and (010) diffraction intensities, especially in the P3HT-end-TAZ:PCBM with an intense decrease, indicate that P3HT-end-TAZ has the lowest crystallinity among the three P3HT blend films due to poor interchain packing by the presence of bulky TAZ end groups as reflected in the decreased UV−vis absorption described above.[43] The intense out-of-plane (100) diffraction peaks of P3HT-end-H/Br:PCBM and P3HT-end-TAZ:PCBM blend films are at $q_z$'s of 0.375 Å$^{-1}$ and 0.368 Å$^{-1}$, corresponding to their $d$ spacings of 16.76 and 17.07 Å, respectively, whereas P3HT-end-OXD:PCBM is at a $q_z$ of 0.380 Å$^{-1}$ ($d$ = 16.54 Å). Moreover, the in-plane (010) diffraction


DOI: 10.1021/acsami.5b03213
ACS Appl. Mater. Interfaces 2015, 7, 20548−20555

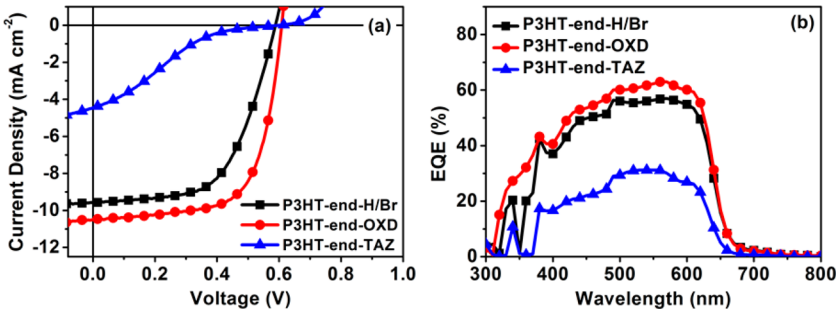


**Figure 5.** (a) $J-V$ characteristics under AM 1.5G illumination with irradiation of 100 mW cm$^{-2}$ and corresponding (b) EQE spectra of the photovoltaic devices based on P3HT:PCBM blend films.

peaks of all the blend films are at a $q_x$ of 1.620 Å$^{-1}$, corresponding to the $\pi-\pi$ stacking distances of all the P3HTs being the same (3.88 Å). Another notably emerged 2D GIWAXS halo at a $q$ of 1.360 Å$^{-1}$ ($d$ = 4.62 Å) in all the blend films is attributed to disordered short-range packing of PCBM, whose diffraction intensities have the same trend as that of the P3HT domains, with the sequence of P3HT-end-OXD > P3HT-end-H/Br ≫ P3HT-end-TAZ. These phenomena of higher crystallinity and closer packing in the P3HT-end-OXD:PCBM blend suggest that OXD end groups with a planar structure can provide similar functionality as nonvolatile additives[44−47] in P3HT:PCBM-based PSCs to assist the interchain interaction of P3HT for an improved degree of crystallinity in P3HT domains as achieved in the solvent annealing treatment,[48] resulting in more efficient pathways with a lower resistance for charge carrier transport to the electrodes.

**Hole Transporting and Photovoltaic Properties.** To further confirm the improvement of hole carrier transport in the blend films with P3HT-end-OXD as the donor relative to the other two P3HTs, hole mobilities across the photoactive layers were measured by applying the SCLC model on the hole-only devices with ITO/PEDOT:PSS/P3HT:PCBM/Au structure, and the results are shown in Figure S4. The hole mobility of the P3HT-end-OXD blend film is increased from P3HT-end-H/Br with a value of 8.68 × 10$^{-6}$ to 1.30 × 10$^{-5}$ cm$^2$ V$^{-1}$ s$^{-1}$ but is significantly higher than that of P3HT-end-TAZ ($\mu_h$ = 4.02 × 10$^{-8}$ cm$^2$ V$^{-1}$ s$^{-1}$) by a factor more than 300, which is also consistent with the GIWAXS result.

The PSCs with the device structure ITO/PEDOT:PSS/P3HT:PCBM/Ca/Al were fabricated to evaluate the effect in photoelectric conversion efficiency by the EDM modification in P3HT chain ends. The $J-V$ curves of the devices with these P3HT:PCBM blends as photoactive layers are shown in Figure 5a, and their photovoltaic parameters are listed in Table 3. For the P3HT-end-TAZ:PCBM blend, the device exhibits a dramatic drop in $J_{sc}$ and FF, leading to the worst PCE of 0.50% among the three P3HTs. However, for the device with P3HT-end-OXD:PCBM, the PCE was remarkably improved to 4.24% as compared to that of P3HT-end-H/Br:PCBM (3.28%), which is mainly due to the enhancement of $J_{sc}$ and FF, from 9.50 mA cm$^{-2}$ and 59.02% to 10.45 mA cm$^{-2}$ and 67.16%, respectively.

**Table 3. Photovoltaic Performance of the Devices Based on the P3HT:PCBM Blend Films**

| polymer | $V_{oc}$ (V) | $J_{sc}$ (mA cm$^{-2}$) | FF (%) | PCE (%)[a] max/avg |
|---|---|---|---|---|
| P3HT-end-H/Br | 0.59 | 9.50 | 59.02 | 3.28/3.17 |
| P3HT-end-OXD | 0.61 | 10.45 | 67.16 | 4.24/4.10 |
| P3HT-end-TAZ | 0.60 | 4.39 | 19.18 | 0.50/0.45 |

[a]Maximum and average of power conversion efficiencies of the PSCs. The average value was calculated from at least five devices.

In accordance with the detailed analyses above, the enhanced $J_{sc}$ in the device with P3HT-end-OXD:PCBM can be attributed to the improvement of P3HT-end-OXD in absorption coefficient, exciton lifetime, and crystallinity in the blend film. In addition, its series resistance ($R_s$) of 6.40 Ω cm$^2$ lower than that with P3HT-end-H/Br ($R_s$ = 14.56 Ω cm$^2$) and P3HT-end-TAZ ($R_s$ = 577.81 Ω cm$^2$) can also support the significant increase in FF value and provide more efficient charge carrier transport pathways within the photoactive layer.[49,50] Therefore, in the P3HT-end-OXD-based device, more photoexcitons can be created and then are able to dissociate to electron−hole pairs after migration to the D−A interface. Finally, the separated charge carriers can favorably transport to the electrodes, resulting in the positive contribution to the photocurrent of PSCs, in which the better performance can also be manifested by EQE measurement in the device with P3HT-end-OXD as a donor. As shown in Figure 5b, the EQE of the device with P3HT-end-OXD is 49 to 63% in the range of 420 to 620 nm, which is higher than those of P3HT-end-H/Br (43 to 57%) and P3HT-end-TAZ (20 to 31%).

## CONCLUSION

In this work, we have presented two end-functionalized P3HTs with the EDM modification in chain ends of common uncapped P3HT. In comparison with the uncapped P3HT, the end-functionalized P3HT with the planar OXD end groups not only can provide multiple functionalities to promote it with a higher absorption coefficient, slightly lower HOMO level, and longer exciton lifetime but also can increase chain ordering without a change of extent of phase separation in the blend film with PCBM for effective charge carrier transport, which are advantageous for improving the PSC performance. BHJ photovoltaic devices by using P3HT-end-H/Br, P3HT-end-OXD, and P3HT-end-TAZ as the donor and PCBM as the acceptor exhibit PCEs of 3.28%, 4.24%, and 0.50%, respectively. These results demonstrate that the type of polymer chain end is also a critical factor in PSC performance, but the structural defect of bromine chain ends can be tailored via end-capping with functional EDMs. However, the efficacy depends on the structure of EDM, such as size and planarity. Hence, the success of the fine modification in P3HT might also provide a promising route for other polymers for enhancement of PSC performance.


DOI: 10.1021/acsami.5b03213
ACS Appl. Mater. Interfaces 2015, 7, 20548−20555

## ■ ASSOCIATED CONTENT

### Supporting Information

The Supporting Information is available free of charge on the ACS Publications website at DOI: 10.1021/acsami.5b03213.

Synthetic procedures, XPS analysis for end groups of P3HTs, UPS spectra of P3HTs, DFT calculation for energy-minimized conformation of P3HTs by simplified model, and hole-only devices of P3HT:PCBM blend films (PDF)

## ■ AUTHOR INFORMATION


### Corresponding Author

*E-mail: sachen@che.nthu.edu.tw.


### Notes

The authors declare no competing financial interest.

## ■ ACKNOWLEDGMENTS

This work was supported by the Ministry of Science and Technology of Taiwan for the financial aid through project MOST-102-2221-E-0070131, MOST-103-2221-E-007-004, and MOST-103-2633-M-007-002. The GIWAXS performed at beamline 17A1, National Synchrotron Radiation Research Center (NSRRC), Hsinchu, Taiwan. The authors gratefully acknowledge Dr. Jey-Jau Lee and Ching-Che Kao for the assistance during the experiments at the 4-circle X-ray Diffractometer Station.

## ■ REFERENCES


(1) Facchetti, A. π-Conjugated Polymers for Organic Electronics and Photovoltaic Cell Applications. *Chem. Mater.* **2011**, *23*, 733−758.

(2) Arias, A. C.; MacKenzie, J. D.; McCulloch, I.; Rivnay, J.; Salleo, A. Materials and Applications for Large Area Electronics: Solution-Based Approaches. *Chem. Rev.* **2010**, *110*, 3−24.

(3) Sun, D.-M.; Timmermans, M. Y.; Tian, Y.; Nasibulin, A. G.; Kauppinen, E. I.; Kishimoto, S.; Mizutani, T.; Ohno, Y. Flexible High-Performance Carbon Nanotube Integrated Circuits. *Nat. Nanotechnol.* **2011**, *6*, 156−161.

(4) Sirringhaus, H.; Brown, P. J.; Friend, R. H.; Nielsen, M. M.; Bechgaard, K.; Langeveld-Voss, B. M. W.; Spiering, A. J. H.; Janssen, R. A. J.; Meijer, E. W.; Herwig, P.; de Leeuw, D. M. Two-Dimensional Charge Transport in Self-Organized, High-Mobility Conjugated Polymers. *Nature* **1999**, *401*, 685−688.

(5) Ma, W.; Yang, C.; Gong, X.; Lee, K.; Heeger, A. J. Thermally Stable, Efficient Polymer Solar Cells with Nanoscale Control of the Interpenetrating Network Morphology. *Adv. Funct. Mater.* **2005**, *15*, 1617−1622.

(6) Liao, S.-H.; Li, Y.-L.; Jen, T.-H.; Cheng, Y.-S.; Chen, S.-A. Multiple Functionalities of Polyfluorene Grafted with Metal Ion-Intercalated Crown Ether as an Electron Transport Layer for Bulk-Heterojunction Polymer Solar Cells: Optical Interference, Hole Blocking, Interfacial Dipole, and Electron Conduction. *J. Am. Chem. Soc.* **2012**, *134*, 14271−14274.

(7) McCullough, R. D.; Lowe, R. D.; Jayaraman, M.; Anderson, D. L. Design, Synthesis, and Control of Conducting Polymer Architectures: Structurally Homogeneous Poly(3-alkylthiophenes). *J. Org. Chem.* **1993**, *58*, 904−912.

(8) Chen, T.-A.; Wu, X.; Rieke, R. D. Regiocontrolled Synthesis of Poly(3-alkylthiophenes) Mediated by Rieke Zinc: Their Characterization and Solid-State Properties. *J. Am. Chem. Soc.* **1995**, *117*, 233−244.

(9) Loewe, R. S.; Ewbank, P. C.; Liu, J.; Zhai, L.; McCullough, R. D. Regioregular, Head-to-Tail Coupled Poly(3-alkylthiophenes) Made Easy by the GRIM Method: Investigation of the Reaction and the Origin of Regioselectivity. *Macromolecules* **2001**, *34*, 4324−4333.

(10) Osaka, I.; McCullough, R. D. Advances in Molecular Design and Synthesis of Regioregular Polythiophenes. *Acc. Chem. Res.* **2008**, *41*, 1202−1214.

(11) Liu, J.; Tanaka, T.; Sivula, K.; Alivisatos, A. P.; Fréchet, J. M. J. Employing End-Functional Polythiophene to Control the Morphology of Nanocrystal-Polymer Composites in Hybrid Solar Cells. *J. Am. Chem. Soc.* **2004**, *126*, 6550−6551.

(12) Chang, J.-F.; Clark, J.; Zhao, N.; Sirringhaus, H.; Breiby, D. W.; Andreasen, J. W.; Nielsen, M. M.; Giles, M.; Heeney, M.; McCulloch, I. Molecular-Weight Dependence of Interchain Polaron Delocalization and Exciton Bandwidth in High-Mobility Conjugated Polymers. *Phys. Rev. B: Condens. Matter Mater. Phys.* **2006**, *74*, 115318/1−115318/12.

(13) Kim, Y.; Cook, S.; Kirkpatrick, J.; Nelson, J.; Durrant, J. R.; Bradley, D. D. C.; Giles, M.; Heeney, M.; Hamilton, R.; McCulloch, I. Effect of the End Group of Regioregular Poly(3-hexylthiophene) Polymers on the Performance of Polymer/Fullerene Solar Cells. *J. Phys. Chem. C* **2007**, *111*, 8137−8141.

(14) Kim, J. S.; Lee, Y.; Lee, J. H.; Park, J. H.; Kim, J. K.; Cho, K. High-Efficiency Organic Solar Cells Based on End-Functional-Group-Modified Poly(3-hexylthiophene). *Adv. Mater.* **2010**, *22*, 1355−1360.

(15) Lee, J. U.; Jung, J. W.; Emrick, T.; Russell, T. P.; Jo, W. H. Synthesis of $C_{60}$-end Capped P3HT and Its Application for High Performance of P3HT/PCBM Bulk Heterojunction Solar Cells. *J. Mater. Chem.* **2010**, *20*, 3287−3294.

(16) Park, J. K.; Jo, J.; Seo, J. H.; Moon, J. S.; Park, Y. D.; Lee, K.; Heeger, A. J.; Bazan, G. C. End-Capping Effect of a Narrow Bandgap Conjugated Polymer on Bulk Heterojunction Solar Cells. *Adv. Mater.* **2011**, *23*, 2430−2435.

(17) Li, G.; Zhu, R.; Yang, Y. Polymer Solar Cells. *Nat. Photonics* **2012**, *6*, 153−161.

(18) Yang, X.; Loos, J. Toward High-Performance Polymer Solar Cells: The Importance of Morphology Control. *Macromolecules* **2007**, *40*, 1353−1362.

(19) Günes, S.; Neugebauer, H.; Sariciftci, N. S. Conjugated Polymer-Based Organic Solar Cells. *Chem. Rev.* **2007**, *107*, 1324−1338.

(20) Thompson, B. C.; Fréchet, J. M. J. Polymer-Fullerene Composite Solar Cells. *Angew. Chem., Int. Ed.* **2008**, *47*, 58−77.

(21) Shao, Y.; Yang, Y. Efficient Organic Heterojunction Photovoltaic Cells Based on Triplet Materials. *Adv. Mater.* **2005**, *17*, 2841−2844.

(22) González, D. M.; Körstgens, V.; Yao, Y.; Song, L.; Santoro, G.; Roth, S. V.; Müller-Buschbaum, P. Improved Power Conversion Efficiency of P3HT:PCBM Organic Solar Cells by Strong Spin-Orbit Coupling-Induced Delayed Fluorescence. *Adv. Energy Mater.* **2015**, *5*, 1401770/1−1401770/10.

(23) Huang, S.-P.; Liao, J.-L.; Tseng, H.-E.; Jen, T.-H.; Liou, J.-Y.; Chen, S.-A. Enhanced Photovoltaic Cells Efficiency *via* Incorporation of High Electron-Deficient Oxadiazole Moieties on Side Chains of Poly(phenylene vinylene)s and Poly(fluorene)s. *Synth. Met.* **2006**, *156*, 949−953.

(24) Chen, S.-H.; Su, A.-C.; Chen, S.-A. Noncrystalline Phases in Poly(9,9-di-n-octyl-2,7-fluorene). *J. Phys. Chem. B* **2005**, *109*, 10067−10072.

(25) Hung, M.-C.; Liao, J.-L.; Chen, S.-A.; Chen, S.-H.; Su, A.-C. Fine Tuning the Purity of Blue Emission from Polydioctylfluorene by End-Capping with Electron-Deficient Moieties. *J. Am. Chem. Soc.* **2005**, *127*, 14576−14577.

(26) Chen, P.-Y.; Rassamesard, A.; Hung, M.-C.; Chen, H.-L.; Chen, S.-A. $C_\beta$ Conformer Formation in Poly(9,9-dioctylfluorene) Single Chains Facilitated by Endcapping with an Electron Deficient Moiety. *RSC Adv.* **2014**, *4*, 14365−14368.

(27) Iqbal, R.; Zareef, M.; Ahmed, S.; Zaidi, J. H.; Khan, K. M.; Arfan, M.; Shafique, M.; Shahzad, S. A. A Convenient Syntheses and Antibacterial Activities of Symmetrical and Unsymmetrical 2, 5-Disubstitutded-1, 3, 4-Oxadiazoles. *J. Chem. Soc. Pak.* **2006**, *28*, 165−168.

(28) Choi, J.; Lee, B.; Kim, J. H. Synthesis and Electroluminescent Properties of π-Conjugated Copolymer Based on 10-Hexylphenothiazine and Aromatic 1,2,4-Triazole. *Synth. Met.* **2009**, *159*, 1922−1927.




DOI: 10.1021/acsami.5b03213
*ACS Appl. Mater. Interfaces* 2015, 7, 20548−20555

(29) Jeffries-EL, M.; Sauvé, G.; McCullough, R. D. In-Situ End Group Functionalization of Regioregular Poly(3-alkylthiophene) Using the Grignard Metathesis Polymerization Method. *Adv. Mater.* **2004**, *16*, 1017−1019.
(30) Frisch, M. J.; Trucks, G. W.; Schlegel, H. B.; Scuseria, G. E.; Robb, M. A.; Cheeseman, J. R.; Scalmani, G.; Barone, V.; Mennucci, B.; Petersson, G. A.; Nakatsuji, H.; Caricato, M.; Li, X.; Hratchian, H. P.; Izmaylov, A. F.; Bloino, J.; Zheng, G.; Sonnenberg, J. L.; Hada, M.; Ehara, M.; Toyota, K.; Fukuda, R.; Hasegawa, J.; Ishida, M.; Nakajima, T.; Honda, Y.; Kitao, O.; Nakai, H.; Vreven, T.; Montgomery, J. A.; Peralta, J. E.; Ogliaro, F.; Bearpark, M.; Heyd, J. J.; Brothers, E.; Kudin, K. N.; Staroverov, V. N.; Kobayashi, R.; Normand, J.; Raghavachari, K.; Rendell, A.; Burant, J. C.; Iyengar, S. S.; Tomasi, J.; Cossi, M.; Rega, N.; Millam, J. M.; Klene, M.; Knox, J. E.; Cross, J. B.; Bakken, V.; Adamo, C.; Jaramillo, J.; Gomperts, R.; Stratmann, R. E.; Yazyev, O.; Austin, A. J.; Cammi, R.; Pomelli, C.; Ochterski, J. W.; Martin, R. L.; Morokuma, K.; Zakrzewski, V. G.; Voth, G. A.; Salvador, P.; Dannenberg, J. J.; Dapprich, S.; Daniels, A. D.; Farkas, O.; Foresman, J. B.; Ortiz, J. V.; Cioslowski, J.; Fox, D. J. *Gaussian 09*, revision A.02; Gaussian, Inc.: Wallingford, CT, 2009.
(31) Shrotriya, V.; Yao, Y.; Li, G.; Yang, Y. Effect of Self-Organization in Polymer/Fullerene Bulk Heterojunctions on Solar Cell Performance. *Appl. Phys. Lett.* **2006**, *89*, 063505/1−063505/3.
(32) Kim, Y.; Cook, S.; Tuladhar, S. M.; Choulis, S. A.; Nelson, J.; Durrant, J. R.; Bradley, D. D. C.; Giles, M.; McCulloch, I.; Ha, C.-S.; Ree, M. A Strong Regioregularity Effect in Self-Organizing Conjugated Polymer Films and High-Efficiency Polythiophene:Fullerene Solar Cells. *Nat. Mater.* **2006**, *5*, 197−203.
(33) Woo, C. H.; Thompson, B. C.; Kim, B. J.; Toney, M. F.; Fréchet, J. M. J. The Influence of Poly(3-hexylthiophene) Regioregularity on Fullerene-Composite Solar Cell Performance. *J. Am. Chem. Soc.* **2008**, *130*, 16324−16329.
(34) Ballantyne, A. M.; Chen, L.; Dane, J.; Hammant, T.; Braun, F. M.; Heeney, M.; Duffy, W.; McCulloch, I.; Bradley, D. D. C.; Nelson, J. The Effect of Poly(3-hexylthiophene) Molecular Weight on Charge Transport and the Performance of Polymer:Fullerene Solar Cells. *Adv. Funct. Mater.* **2008**, *18*, 2373−2380.
(35) Brown, P. J.; Thomas, D. S.; Köhler, A.; Wilson, J. S.; Kim, J.-S.; Ramsdale, C. M.; Sirringhaus, H.; Friend, R. H. Effect of Interchain Interactions on the Absorption and Emission of Poly(3-hexylthiophene). *Phys. Rev. B: Condens. Matter Mater. Phys.* **2003**, *67*, 064203/1−064203/16.
(36) Wang, G.; Swensen, J.; Moses, D.; Heeger, A. J. Increased Mobility from Regioregular Poly(3-hexylthiophene) Field-effect Transistors. *J. Appl. Phys.* **2003**, *93*, 6137−6141.
(37) Lim, T.-S.; Hsiang, J.-C.; White, J. D.; Hsu, J. H.; Fan, Y. L.; Lin, K. F.; Fann, W. S. Single Short-chain Conjugated Polymer Studied with Optical Spectroscopy: A Donor-acceptor System. *Phys. Rev. B: Condens. Matter Mater. Phys.* **2007**, *75*, 165204/1−165204/9.
(38) Bulle-Lieuwma, C. W. T.; van Gennip, W. J. H.; van Duren, J. K. J.; Jonkheijm, P.; Janssen, R. A. J.; Niemantsverdriet, J. W. Characterization of Polymer Solar Cells by TOF-SIMS Depth Profiling. *Appl. Surf. Sci.* **2003**, *203*−*204*, 547−550.
(39) Prosa, T. J.; Winokur, M. J.; Moulton, J.; Smith, P.; Heeger, A. J. X-ray Structural Studies of Poly(3-alkylthiophenes): An Example of an Inverse Comb. *Macromolecules* **1992**, *25*, 4364−4372.
(40) Zhang, Z.-G.; Min, J.; Zhang, S.; Zhang, J.; Zhang, M.; Li, Y. Alkyl Chain Engineering on a Dithieno[3,2-*b*:2′,3′-*d*]silole-alt-dithienylthiazolo[5,4-*d*]thiazole Copolymer Toward High Performance Bulk Heterojunction Solar Cells. *Chem. Commun.* **2011**, *47*, 9474−9476.
(41) Zuo, G.; Li, Z.; Zhang, M.; Guo, X.; Wu, Y.; Zhang, S.; Peng, B.; Wei, W.; Hou, J. Influence of the Backbone Conformation of Conjugated Polymers on Morphology and Photovoltaic Properties. *Polym. Chem.* **2014**, *5*, 1976−1981.
(42) Yang, X.; Loos, J.; Veenstra, S. C.; Verhees, W. J. H.; Wienk, M. M.; Kroon, J. M.; Michels, M. A. J.; Janssen, R. A. J. Nanoscale Morphology of High-Performance Polymer Solar Cells. *Nano Lett.* **2005**, *5*, 579−583.
(43) Shao, M.; Keum, J.; Chen, J.; He, Y.; Chen, W.; Browning, J. F.; Jakowski, J.; Sumpter, B. G.; Ivanov, I. N.; Ma, Y.-Z.; Rouleau, C. M.; Smith, S. C.; Geohegan, D. B.; Hong, K.; Xiao, K. The Isotopic Effects of Deuteration on Optoelectronic Properties of Conducting Polymers. *Nat. Commun.* **2014**, *5*, 1−11.
(44) Yao, Y.; Hou, J.; Xu, Z.; Li, G.; Yang, Y. Effects of Solvent Mixtures on the Nanoscale Phase Separation in Polymer Solar Cells. *Adv. Funct. Mater.* **2008**, *18*, 1783−1789.
(45) Jeong, S.; Kwon, Y.; Choi, B.-D.; Kwak, G.; Han, Y. S. Effects of Nematic Liquid Crystal Additives on the Performance of Polymer Solar Cells. *Macromol. Chem. Phys.* **2010**, *211*, 2474−2479.
(46) Jeong, S.; Woo, S.-H.; Lyu, H.-K.; Kim, C.; Kim, W. H.; Han, Y. S. Improved Photovoltaic Properties of Polymer Solar Cells with a Phenyl Compound as an Additive. *J. Nanosci. Nanotechnol.* **2014**, *14*, 5988−5992.
(47) Heo, S. W.; Baek, K. H.; Song, H. J.; Lee, T. H.; Moon, D. K. Improved Performance of P3HT:PCBM-Based Solar Cells Using Nematic Liquid Crystals as a Processing Additive under Low Processing Temperature Conditions. *Macromol. Mater. Eng.* **2014**, *299*, 353−360.
(48) Li, G.; Yao, Y.; Yang, H.; Shrotriya, V.; Yang, G.; Yang, Y. "Solvent Annealing" Effect in Polymer Solar Cells Based on Poly(3-hexylthiophene) and Methanofullerenes. *Adv. Funct. Mater.* **2007**, *17*, 1636−1644.
(49) Chi, D.; Qu, S.; Wang, Z.; Wang, J. High Efficiency P3HT:PCBM Solar Cells with an Inserted PCBM Layer. *J. Mater. Chem. C* **2014**, *2*, 4383−4387.
(50) Qi, B.; Wang, J. Fill Factor in Organic Solar Cells. *Phys. Chem. Chem. Phys.* **2013**, *15*, 8972−8982.


DOI: 10.1021/acsami.5b03213
*ACS Appl. Mater. Interfaces* 2015, 7, 20548−20555